

Evidence for generalized Kirchhoff's law from angle-resolved electroluminescence of high efficiency silicon solar cells

L. Ferraioli and P. Maddalena^{a)}

INFN-COHERENTIA, Dipartimento di Scienze Fisiche, Università di Napoli "Federico II," Via Cintia, I-80126 Napoli, Italy

E. Massera and A. Parretta

ENEA Centro Ricerche Portici, Località Granatello, I-80055 Portici (Na), Italy

M. A. Green

Centre for Third Generation Photovoltaics, University of New South Wales, Sydney NSW 2052, Australia

A. Wang and J. Zhao

Centre for Photovoltaic Engineering, University of New South Wales, Sydney NSW 2052, Australia

(Received 17 February 2004; accepted 19 July 2004)

The angular distribution of infrared radiation, emitted by high efficiency single-crystalline silicon solar cells, was analyzed. Measurements were performed on cells with planar and inverted-pyramids surfaces, both showing integral emissions that approach the cosine function in the 0° – 90° interval. Textured cell maintains the cosine distribution at the different wavelengths; planar device shows a distribution, which deviates from the cosine function at increasing wavelength. Correspondence between emission and absorption properties was demonstrated valid as a function of emission/absorption angle. From the angular distribution of electroluminescence light, the devices absorption properties for incident light with directions different from the surface normal were estimated. © 2004 American Institute of Physics. [DOI: 10.1063/1.1795361]

Due to the indirect band gap structure of crystalline silicon (*c*-Si), the band-edge phonon-assisted photoluminescence (PL) from bulk *c*-Si material has usually very low efficiency, with a measured internal quantum efficiency of 10^{-6} – 10^{-4} and an external quantum efficiency of 10^{-7} – 10^{-5} .^{1,2} Hence, most of past research in silicon light emission has taken an alternative approach with quantum confinement effects in nanosized silicon crystals.^{3,4} Devices reported include those based on porous silicon,^{3–6} silicon nanocrystals in SiO₂,^{7,8} amorphous-Si/SiO₂ superlattices structures⁹ and Si/Si_{1-x}Ge_x cascade quantum wells.¹⁰

Greatly improved band-edge emission from bulk *c*-Si has been recently demonstrated¹¹ using a bulk silicon light emitting diode (LED) structure based on high efficiency PERL (passivated emitter, rear locally diffused) silicon solar cells of efficiency up to 24.7%.^{12,13} The excellent surface passivation in these devices has significantly reduced the nonradiative recombination process. The light trapping scheme with front inverted pyramids and a rear surface mirror, which was designed to improve the absorption of the weakly absorbed long-wavelength light, also improves the light escaping from the device, as predicted by Kirchhoff's law,¹⁴ with power conversion efficiency up to 1% demonstrated.¹¹ Using a *c*-Si LED and a *c*-Si solar cell as a detector, a high optical coupling quantum efficiency of 0.18% was also demonstrated.¹⁵ A further surface passivation improvement has recently resulted in over 10% photoluminescence quantum efficiency.¹⁶

The main purpose of this work is to study the angular distribution pattern of electroluminescence (EL) emission from these silicon solar cells at room temperature. The EL

emission pattern of the solar cells can be used to know, following a generalized version of Kirchhoff's law, its performance under light incident from a generic direction to the top surface. This fact is remarkable since the characterization of a solar cell is typically performed with incident light perpendicular to the top surface of cell, giving only a partial knowledge of the cell performance in operation outdoors. In order to confirm the generalized version of Kirchhoff's law at any angle of emission/absorption, angle-resolved absorption intensity measurements on both planar and textured devices have been also carried out.

The short circuit current of a solar cell can be written as:

$$I_{sh}(\lambda, \vartheta, \varphi) = q[1 - R_s(\lambda, \vartheta, \varphi)] \frac{I_0(\lambda)\lambda}{hc} \times \alpha_{eh}(\lambda)P(\lambda, \vartheta, \varphi)S \cos(\vartheta), \quad (1)$$

where q is the elementary charge, $I_0(\lambda)$ is the light intensity incident on the cell, R_s is the top surface reflectance, S is the surface area of the cell, $\alpha_{eh}(\lambda)$ is the part of absorption coefficient due to transitions which generate electron-hole pairs, $P(\lambda, \vartheta, \varphi)$ is a quantity that keeps trace of multiple reflections and has not, in general, an analytical expression, and $\cos(\vartheta)$ is a geometric factor. In the above expression we have assumed monochromatic light of wavelength λ and direction of incidence identified by the angles θ and φ , the zenithal and azimuthal angles, respectively. For a high quality solar cell, defined as one that collects virtually all internally generated electron-hole pairs, the generalized Kirchhoff's law states that the light emission properties of the cell are closely related to its absorption properties.^{11,17} Indeed, starting from the Planck's radiation law, the Kirchhoff's law can be derived, which states that at thermal equilibrium and for each wavelength the emissivity of a body equals its

^{a)} Author to whom correspondence should be addressed; electronic mail: maddalena@na.infn.it

absorptivity.¹⁸ Based on microscopic transition probabilities and on the principle of detailed balance, absorption and emission rates can also be calculated for an indirect gap semiconductor, where phonon contribution effects are involved.¹⁹ Even in this latter case, a generalized Planck's law can be formulated, containing the photons chemical potential, which is related to the quasi-Fermi energies of electrons and holes. As a consequence, Kirchhoff's law still applies so it can be generally referred to as the generalized Kirchhoff's law.

Measuring the angular distribution of EL light from the cell we have access to the current given by the cell for light incidence direction characterized by $\vartheta \in [0, \pi/2]$ and $\varphi \in [0, 2\pi]$. Further dividing Eq. (1) by the geometric factor $\cos(\vartheta)$ we can experimentally derive the quantity $P(\lambda, \vartheta, \varphi)$, that otherwise is approachable via a simulation only.

Crystalline-Si PERL solar cells with both planar and inverted pyramids top surfaces were characterized. The cell surface dimensions are both $2 \times 2 \text{ cm}^2$, their thickness is $450 \mu\text{m}$. In textured cells, surface texture is formed by anisotropic etching of the (100) oriented silicon surface to produce inverted pyramids with a base size of $\sim 10 \mu\text{m}$, distributed in a regular square array on the top surface of the device. They play an important role in reducing surface reflection, due to multiple reflections of light on the pyramid sides before coupling into silicon, and in increasing internal absorptance by trapping weakly absorbed long wavelength light within the cell. More details on the cells structure can be found in Refs. 12 and 13. The devices, glued onto a plastic table, were electrically connected with silver paint on the top and rear surfaces. The cell edges were covered during measurement, to obtain the front emission angular distribution only.

In order to investigate the light emission angular distribution, we used a two-axis rotation stage for orienting the sample at discrete values of the zenithal and azimuthal angles, while a Ge detector was held fixed on the optical axis at a certain distance, depending on the type of measurements.

The centering of the cell with respect to the detector was obtained by three linear translation stages. For spectral measurements an interferential filter of $\sim 30 \text{ nm}$ bandwidth was placed in front of the Ge detector. The investigated spectral range corresponds to the wavelength interval of the cells emission (1000–1300 nm).¹³ The device was powered by a direct current in the range of 30–300 mA, modulated at $\sim 38 \text{ Hz}$; the emitted light was detected by the Ge photodiode, whose signal was analyzed by lock-in technique.

Measurements were carried out at different azimuth angles, with a 0° – 90° extension of the zenith angle. Both the textured device and the planar one have shown an azimuth angle symmetric emission. Figure 1(a) shows the textured cell results. The shape of angular emission intensity follows the cosine function of zenith angle for the wavelengths analyzed, as a consequence of the randomizing effect produced by texture on light propagation into the device. The results for planar cell are shown in Fig. 1(b). The shape of angular emission shows a clear curve distortion with respect to the cosine function. This peculiarity is amplified as the wavelength of emitted light increases. The more efficient emission at high zenithal angles is equivalent to a more efficient carrier collection, a consequence of the increased refraction angle and reduced penetration depth of radiation, as will be

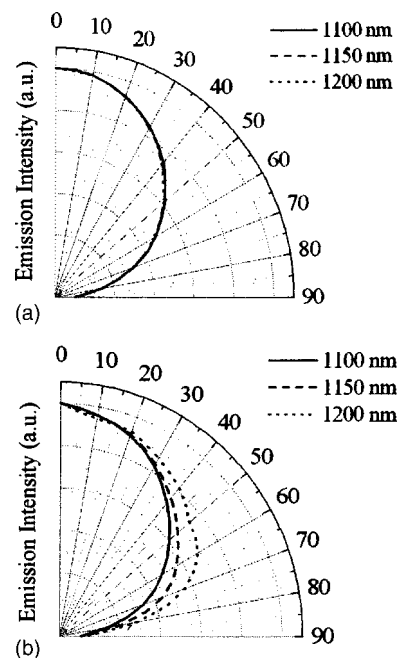


FIG. 1. Spectral emission curves for a textured cell (a) and a planar cell (b).

later discussed when measurements on the light absorption properties will be presented.

The correspondence between absorption and emission properties, as predicted by the generalized Kirchhoff's law,¹⁷ has been tested for angular resolved measurements in non-stationary conditions. The absorption measurements were made in the 0° – 90° interval at steps of 5° , at the peak wavelength (1150 nm) of the emission curve of the cell. The light emitted by a QTH lamp, filtered by a 30 nm bandpass optical filter and intensity modulated by a mechanical chopper, was incident on the cell placed on the two axis rotation stage as in emission measurements. The generated photocurrent, measured by a lock-in amplifier, gives a direct estimation of the absorption, since only the absorbed photons generate charge carriers and, hence, contribute to the measured signal. The absorption curves are compared with the emission curves for both devices in Fig. 2. The correspondence between emission and absorption at any angle of observation appears very satisfactory.

In Fig. 3 we represent the quantity:

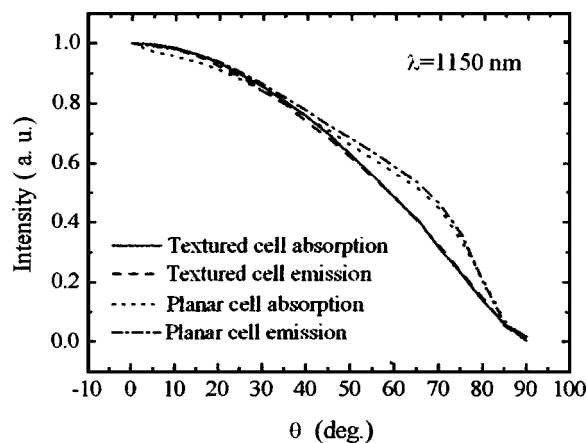


FIG. 2. Comparison of angular emission and absorption for a textured cell and a planar.

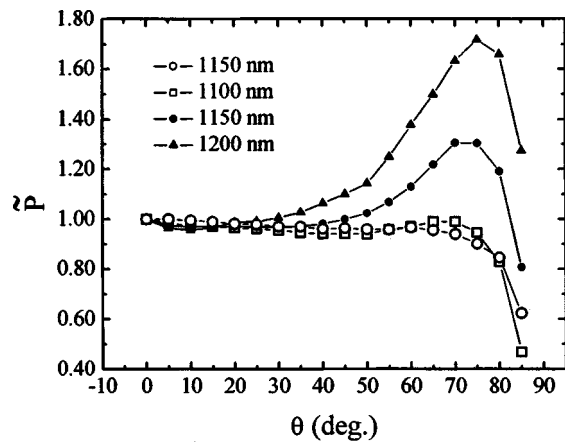


FIG. 3. \tilde{P} variation with zenith angle for textured cell (empty symbols) and planar cell (filled symbols).

$$\tilde{P}(\lambda, \theta, \varphi) = [1 - R_s(\lambda, \theta, \varphi)]P(\lambda, \theta, \varphi) \quad (2)$$

as a function of the zenith angle θ , normalized to the value assumed at $\theta=0$, for both the textured and planar cells. The quantity \tilde{P} , which represents the real absorption properties of the cell free from the geometric factor $\cos(\theta)$, shows a good degree of constancy until $\theta=70^\circ$ for the textured cell. For zenith angles greater than 70° device absorption properties start to get worse due to surface reflection. The same trend of Fig. 3 is observed for light absorbed in the wavelength interval from 1100 to 1300 nm.

The results show again that the cell inverted pyramids texture is capable of randomizing the incident light, making its absorption properties independent on the incidence angle and wavelength of incident light.

In Fig. 3 the quantity \tilde{P} is also shown for the plane surface cell at three different wavelengths. The 1100 nm curve shows a constant trend until 70° is reached. The 1150 nm and the 1200 nm curves start to increase from unit at $\theta=50^\circ$ and $\theta=30^\circ$, respectively, and they reach a maximum at $\theta=70^\circ-80^\circ$. The three curves drop to zero at the highest angles due to surface reflection. The absorption of light at wavelengths longer than 1100 nm is critically dependent on the optical path of light in the cell. Increasing the angle of incidence, also increases the light path in the device and the cell absorption capability. The trend shown by the curves of Fig. 3 demonstrates the enhanced absorption capa-

bility of planar c-Si cell with respect to normal incidence in the near-infrared wavelength range.²⁰ The same feature was not present in the inverted pyramids cell due to surface texture presence, that effectively homogenizes the device absorption capability with respect to incidence angle and wavelength in the near infrared wavelength range.

In conclusion, the optical emission angular distribution properties of high efficiency silicon solar cells have been investigated. The front emission has shown generally a cosine distribution respect to the zenith angle. For planar cells a sensible distortion from the cosine distribution has been observed at $\lambda=1200$ nm. The generalized Kirchhoff's law for the correspondence between absorption and emission has been verified in the $0^\circ-90^\circ$ interval. From the angular distribution of light emitted by the cells, we were able to estimate the devices response to incident light with directions different from the surface normal and at different wavelengths near the gap.

¹O. King and D. G. Hall, Phys. Rev. B **50**, 10661 (1994).

²T. C. Ong, K. W. Terrill, S. Tam, and C. Hu, IEEE Electron Device Lett. **EDL-4**, 460 (1983).

³L. T. Canham, Appl. Phys. Lett. **57**, 1046 (1990).

⁴S. S. Lyer and Y. H. Xie, Science **260**, 40 (1993).

⁵K. D. Hirschman, L. Tsybeskov, S. P. Duttagupta, and P. M. Fauchet, Nature (London) **384**, 338 (1996).

⁶P. Schmuki, L. E. Erickson, and D. J. Lockwood, Phys. Rev. Lett. **80**, 4060 (1998).

⁷Y. Q. Wang, G. L. Kong, W. D. Chen, H. W. Diao, C. Y. Chen, S. B. Zhang, and X. B. Liao, Appl. Phys. Lett. **81**, 4174 (2002).

⁸L. Pavesi, L. Dal Negro, C. Mazzoleni, G. Franzó, and F. Priolo, Nature (London) **408**, 440 (2000).

⁹Z. H. Lu, D. J. Lockwood, and J. M. Baribeau, Nature (London) **378**, 258 (1995).

¹⁰G. Dehlinger, L. Diehl, U. Gennser, H. Sigg, J. Faist, K. Ensslin, D. Grutzmacher, and E. Muller, Science **290**, 2277 (2000).

¹¹M. A. Green, J. Zhao, A. Wang, P. J. Reece, and M. Gal, Nature (London) **412**, 805 (2001).

¹²A. Wang, J. Zhao, and M. A. Green, Appl. Phys. Lett. **57**, 602 (1990).

¹³J. Zhao, A. Wang, and M. A. Green, Prog. Photovoltaics **7**, 471 (1999).

¹⁴G. R. Kirchhoff, Ann. D. Phys. **109**, 275 (1860) (in German).

¹⁵J. Zhao, M. A. Green, and A. Wang, J. Appl. Phys. **92**, 2977 (2002).

¹⁶T. Trupke, J. Zhao, A. Wang, R. Corkish, and M. A. Green, Appl. Phys. Lett. **82**, 2996 (2003).

¹⁷P. Würfel, J. Phys. C **15**, 3967 (1982).

¹⁸L. D. Landau and E. M. Lifshitz, *Statistical Physics*, 3rd Ed., (Butterworth-Heinemann, Oxford, 1980), Part 1.

¹⁹P. Würfel, S. Finkbeiner, and E. Daub, Appl. Phys. A: Mater. Sci. Process. **60**, 67 (1995).

²⁰A. Parretta, P. Grillo, and M. Tucci, Mater. Sci. Eng., B **102**, 179 (2003).